Structure of the Solvated Strontium and Barium Ions in Aqueous, Dimethyl Sulfoxide and Pyridine Solution, and Crystal Structure of Strontium and Barium Hydroxide Octahydrate

Ingmar Persson*, Magnus Sandström**, Haruhiko Yokoyama***, and Monika Chaudhry*

* Department of Chemistry, Swedish University of Agricultural Sciences, P.O. Box 7015, S-750 07 Uppsala, Sweden

** Coordination Chemistry Laboratories, Institute for Molecular Science, Myodaiji, Okazaki 444, Japan

*** Department of Chemistry, Yokohama City University, Seto, Kanazawa-ku, Yokohama 236, Japan

Z. Naturforsch. **50 a**, 21–37 (1995); received November 8, 1994

Dedicated to Prof. Hitoshi Ohtaki on the occasion of his 60th birthday

Single crystal X-ray data, collected at 298 K, are used to redetermine the crystal structure of the non-isomorphic compounds $[Sr(H_2O)_8](OH)_2$ and $[Ba(H_2O)_8](OH)_2$. The eight water oxygen atoms form distorted Archimedean antiprisms around the octahydrated metal ions with mean metal ion-oxygen distances 2.62 and 2.79 Å for strontium and barium, respectively. A second coordination shell of 24 hydrogen-bonded oxygen atoms with mean metal ion-oxygen distances $M \cdots O^{II}$ 4.76 and 4.80 Å, respectively, is observed. The hydroxide ions in both structures have an unusual hydrogen bond arrangement with 5 bonds accepted and one donated.

The structure of the solvated strontium and barium ions in aqueous, dimethyl sulfoxide and pyridine solutions has been studied by means of large angle X-ray scattering and extended X-ray absorption fine structure spectroscopy techniques. In aqueous solution independent determinations of the first-sphere metal-oxygen coordination by the two techniques resulted in the bond lengths Sr–O 2.63 (2) and Ba–O 2.81 (3) Å, and for both metal ions a hydration number of 8.1 (3). The second coordination spheres are very diffuse with only about 13 water molecules at similar $M \cdots O^{II}$ distances as in the crystal structures and 2–3 water molecules closer to the metal ions. In dimethyl sulfoxide solution both ions were found to coordinate 6.0 (5) solvent molecules with the distances Sr–O 2.54 (1), Sr···S 3.77 (1) Å, and Ba–O 2.76 (1), Ba···S 3.99 (1) Å. For the solvated ions in pyridine solution EXAFS measurements yielded the distances Sr–N 2.57 (2) and Ba–N 2.78 (3) Å, with a probable solvation number of 6.

Correlations of hydration enthalpies and partial molar volumes with experimental M–O bond distances in aqueous solution are used to discuss hydration numbers and bond character for all of the alkaline earth metal ions.

Key words: Barium; Strontium; Hydration; Solvation; Structure.

Introduction

The solvation is important for the chemical properties of metal ions in solution. A qualitative classification of the character and the relative strength of the metal ion-solvent interactions can be made in terms of the electron-pair donor and acceptor properties of the solvent and the metal ion, respectively [1–3]. In continuation of a structural and thermodynamic investigation of a number of anions and cations in some solvents with widely different electron-pair donor properties [4–7], the solvation of strontium and barium ions in water, dimethyl sulfoxide and pyridine solution has been investigated in the present work. The transfer thermodynamic properties for the alkaline earth metal ions from water to these solvents have been reported previously [7, 8]. In the present study the structure of the solvated strontium and barium ions is investigated.

Water is a hard polar and protic solvent with extensive hydrogen bonding. It solvates the hard alkaline-earth metal ions relatively strongly. Dimethyl sulfoxide is aprotic with high dipole moment and permittivity. The solvation of hard metal ions occurs *via* its oxygen atom and is stronger than in water, as

Reprint requests to Dr. Magnus Sandström; Permanent address: Department of Chemistry, Royal Institute of Technology, S-100 44 Stockholm, Sweden.

0932-0784 / 95 / 0100-0021 $ 06.00 © – Verlag der Zeitschrift für Naturforschung, D-72027 Tübingen

shown from the transfer thermodynamics [7]. Pyridine is a fairly soft donor solvent with low dipole moment and permittivity, and consequently, salts of divalent ions have a relatively low solubility in pyridine, even in the cases where a soft and strongly solvated cation is the acceptor [9].

Structure Determination in Solution

Although several crystal structure determinations of hydrated strontium and barium salts have been reported, few attempts have been made to study the solvated ions in solution, mainly because of the experimental difficulties [10]. An attempt has been made to study the hydration of the strontium ion in a 3 molal solution of $Sr(ClO_4)_2$ in D_2O by isotopic substitution [11]. Even though the radial distribution curve showed poor resolution, the direct Fourier transformation of the difference intensity function (Fig. 2 of [11]) displays maxima which should correspond to Sr–O and Sr–D distances of about 2.65 and 3.2–3.3 Å, respectively.

LAXS (large angle X-ray scattering) experiments give a weighted contribution of all interatomic distances in the sample. There is severe overlap between the metal-oxygen (especially Ba–O) distances and the hydrogen-bonded oxygen-oxygen distances for the aqueous solutions. In order to get reliable results on the hydration structure around these metal ions it was necessay to eliminate these back-ground contributions from the bulk water and the perchlorate ions by applying a modification of a previously developed difference procedure [12].

In an extended X-ray absorption fine structure (EXAFS) experiment only the local structure around the absorbing atom contributes to the backscattering of the ejected photoelectron wave. The theoretical expression of the EXAFS intensity in terms of the momentum of the photoelectron wave is usually given as [13a]

$$\chi(k) = \sum N_i |f_i(k)| \exp(-2\sigma^2 k^2) \cdot \exp(-d_i/\varrho) \sin[2kd_i + \varphi_i(k)]/kd_i^2, \quad (1)$$

where N_i is the number of atoms in the ith shell at a distance d_i from the absorbing atom. The backscattering amplitude from this shell is $f_i(k)$ for which the associated phase is $\varphi_i(k)$, and ϱ is the mean free path of the electron. The magnitude of the photoelectron wave vector is given by $k = [8\pi^2 m_e h^{-2}(E - E_0)]$, where E denotes the energy of the incident photoelectron and E_0 the threshold energy, m_e the mass of the electron and h is Planck's constant. The part $\exp(-d_i/\varrho \sin[2kd_i + \varphi_i(k)]/kd_i^2$ of (1), after the Debye-Waller factor $\exp(-2\sigma_i^2 k^2)$ given in the harmonic approximation [13b], is comparable to the $(\sin s d_{ij})/(s d_{ij})$ factor of the theoretical expression for the structure-dependent reduced intensity contribution from a pair interaction between the atoms i and j in the LAXS method [14]

$$i_c(s) = \sum\sum [f_i(s) f_j(s) + \Delta f_i'' \Delta f_j''] \cdot \exp(-l_{ij}^2 s^2/2) \sin(s d_{ij})/s d_{ij}). \quad (2)$$

The comparison shows that the amplitude of the structure-dependent intensity contributions decreases more rapidly in the EXAFS experiment, particularly at longer interatomic distances d. There are also indications that a non-symmetric distribution of the distances gives rise to a more severe damping effect on EXAFS than LAXS intensities [15]. The Debye-Waller factor $\exp(-l_{ij}^2 s^2/2)$ is in the LAXS method often expressed by means of the root-mean-square variation l_{ij}, (assuming a Gaussian distribution) around the mean interatomic distance d_{ij}, the f values are the scattering factors with corrections for anomalous dispersions (of which $\Delta f''$ is the imaginary part), and the magnitude of the wave vector is $s = 4\pi\lambda^{-1}\sin\theta$, where 2θ is the scattering angle and λ the wavelength of the X-ray radiation.

Another difference is the momentum range available, which for the LAXS technique (Mo Kα radiation) normally is $0.3 < s < 16.5$ Å^{-1} because of experimental constraints, while the useful EXAFS region usually covers a range of ca. $3 < k < 15$ Å^{-1}. The lack of low k data and the damping of long-distance intensity contributions allow normally only distinct intramolecular interactions with the absorbing atom to be determined from EXAFS data. On the other hand, the different types of scattering factors $f_i(k)$ and $f_i(s) f_j(s)$ in the EXAFS and LAXS expressions (1) and (2), respectively, can make it easier to distinguish contributions from light atoms in the presence of heavier atoms in the first coordination shell by the EXAFS technique because of its different shape of the amplitude envelopes for light and heavy backscattering elements [13]. This can be useful in studies of overlapping distances in the first coordinating sphere around metal ions, for example hydrated halide complexes [15]. Moreover, with synchrotron radiation lower solute concentrations can be studied, especially for low-absorbing solvents.

For barium compounds there are additional limitations in using the EXAFS technique. At the Ba K absorption edge, 37.41 keV (0.3314 Å), the intensity is too low, and the L_{III} edge at 5.22 keV is followed fairly closely by the L_{II} edge at 5.60 keV [16]. This means that the Ba L_{III} edge EXAFS data are only useful up to about $k = 9$ Å^{-1} (5580 eV), which gives broader peaks in the Fourier transform and lower precision of the barium-ligand distances than in the normal case. The L_I edge cannot be used either because the EXAFS contributions from all L edges overlap in this energy region. Because of these difficulties independent determinations of the coordination of water molecules to the strontium and barium ions in aqueous solution were performed in the present study by a LAXS difference method and by the EXAFS technique.

When interpreting EXAFS data it is often advantageous to use model compounds with similar coordination geometry and known bond distances for an empirical determination of the amplitude, $f_i(k)$, and phase factors, $\varphi_i(k)$, in order to include effects not accounted for in (1). If more detailed analyses are desired of, e.g. non-symmetrical distribution of the distances or multiple scattering, theoretical *ab initio* calculations of the back-scattering parameters are useful [17]. In the present case the crystalline $Sr(H_2O)_8(OH)_2$ and $Ba(H_2O)_8(OH)_2$ compounds with octahydrated strontium and barium ions are suitable [18–20]. However, the old crystal structure determinations by film methods of the strontium and barium compounds [18, 19] have low accuracy. The Sr–O distance given for the octahydrate, 2.60 Å [18], is shorter than the LAXS value, 2.64 Å, reported for eight-coordination in aqueous solution [21]. Therefore, redetermination of the crystal structures was performed in order to use empirically calibrated EXAFS data as a check of the reliability of the results obtained by the LAXS difference procedure. At this time we were not aware of a recent redetermination of the $Ba(H_2O)_8(OH)_2$ compound [20].

In dimethyl sulfoxide solutions of strontium and barium salts, LAXS studies give no severe overlap between the metal ion-solvent and intermolecular solvent-solvent distances, in contrast to the situation for the aqueous solutions. Furthermore, the metal ion-sulfur distances of the solvated metal ions give not only the M–O–S angle but also an independent measure of the number of coordinated dimethyl sulfoxide molecules. EXAFS studies were also performed, although the high absorption of the solvent in this case made it necessary to use high solute concentrations and cells with short pathlengths.

For pyridine solutions, however, only EXAFS measurements were meaningful because of the insufficient solubility of the strontium and barium salts for LAXS studies.

Experimental

Sample Preparations

Strontium and barium trifluoromethanesulfonate, prepared as described in [22], were dissolved in freshly distilled dimethyl sulfoxide, pyridine or water. The composition of the solutions studied is given in Table 1. The solid compounds $Sr(H_2O)_8(OH)_2$ and $Ba(H_2O)_8(OH)_2$ (Merck, analytical reagent) were recrystallized under nitrogen atmosphere by cooling filtered solutions [23] and identified by X-ray powder diffraction methods. For the crystal structure data collections the selected single crystals were fastened with epoxy resin inside thin-walled capillaries which were sealed without delay to avoid formation of carbonates. The aqueous strontium and barium perchlorate

Table 1. Composition in mol dm^{-3} of the solutions studied by LAXS and EXAFS.

Ion	Solvent	$[M^{2+}]$	$[CF_3SO_3^-]$	$[ClO_4^-]$	[Solvent]	V/Å^3	μ/cm^{-1}	Method
Sr^{2+}	Water	0.82		1.64	53.5	2025	8.1	LAXS
Sr^{2+}	Water	0.10	0.20					EXAFS
Sr^{2+}	Me_2SO	1.30	2.60		11.3	1277	15.9	LAXS, EXAFS
Sr^{2+}	Pyridine	0.10	0.20					EXAFS
Ba^{2+}	Water	0.82		1.64	53.5	2025	6.5	LAXS
Ba^{2+}	Water	0.20		0.40				EXAFS (SSRL)
Ba^{2+}	Water	0.20	0.40					EXAFS (SRS)
Ba^{2+}	Me_2SO	1.30	2.60		10.9	1277	12.8	LAXS, EXAFS
Ba^{2+}	Pyridine	0.10	0.20					EXAFS

solutions were prepared by dissolving the corresponding hydroxides in perchloric acid.

Crystal Structure Data

Details of the data collections and treatments are given in Table 2. Cell parameters were obtained from least-squares refinement of 25 centered high-angle reflections ($2\theta > 25°$). For the $Sr(H_2O)_8(OH)_2$ crystal a separate precise unit cell determination was made on an Enraf-Nonius CAD4 instrument which resulted in parameters in acceptable agreement with those from a powder diffraction study [24]. The intensity data were corrected for Lorentz and polarization effects and converted into scaled $|F_0|$ values. A semi-empirical absorption correction [25] obtained by a ψ-scan of selected reflections with χ values $> 70°$, gave a slight improvement of the barium data, but not for strontium. The SHELXTL program system in Siemens PC-version [26] was used for treatment of the data sets collected on a PC-controlled Syntex $P2_1$ diffractometer. Full matrix least-squares refinements were carried out of the model parameters. The function minimized is $\sum w \| F_0 \| - \| F_c \|^2$ with the weighting function w given in Table 2. The scattering factors used were calculated from analytical expressions for the neutral atoms with anomalous dispersion corrections for the barium, strontium and oxygen atoms included [27a].

LAXS Data

A large angle θ–θ diffractometer, described previously [28], was used to measure the Mo-K α (0.7107 Å) X-ray scattering from the free surface of the solutions. The scattered intensity was measured by means of a scintillation counter at ca. 400 discrete θ-values in the region $1° < \theta < 70°$ of the scattering angle 2θ, accumulating at least 10^5 counts twice for each θ-value, which corresponds to a statistical error of less than 0.3%. The amount of Compton scattering reaching the detector was reduced by means of a focusing LiF monochromator.

The data treatment was performed as previously described by means of the KURVLR program [14]. The experimental intensities were normalized to a stoichiometric unit-volume corresponding to one metal atom, using scattering factors for neutral atoms, f, including corrections for anomalous dispersion, $\Delta f'$ and $\Delta f''$, and for the calculated Compton scattering multiplied by an empirical apparatus function, with tabulated values from the same sources as before [12a, 27a]. For the dimethyl sulfoxide solutions the reduced coherent intensity functions, $i_{exp}(s)$, multiplied by the scattering variable $s = (4\pi/\lambda)\sin\theta$, are shown in Figure 1. The corresponding experimental radial distribution functions (RDFs) in the form $D(r) - 4\pi r^2 \varrho_0$,

Table 2. Crystal data and conditions for data collection and treatment of the $[Sr(OH_2)_8](OH)_2$ and $[Ba(OH_2)_8](OH)_2$ structures.

Condition	$[Sr(OH_2)_8](OH)_2$	$[Ba(OH_2)_8](OH)_2$
Diffractometer	Syntex $P2_1$	Syntex $P2_1$
T/K	298	298
Space group	$P4/ncc$ (No. 130)[a]	$P2_1/n$ (No. 14)[b]
Crystal class	Tetragonal	Monoclinic
a/Å	9.0168(3)[c]	9.301(2)
b/Å	9.0168(3)[c]	9.289(2)
c/Å	11.6090(6)[c]	11.848(4)
α/°	90	90
β/°	90	98.94(3)
γ/°	90	90
V/Å	943.84(6)	1011.2(5)
Z	4	4
D_{calc}/g cm^{-3}	1.870	2.072
D_{exp}	$1.88\frac{2}{5}^{3}$	2.086(5)[18]
$F(000)$	544	616
Data collection		
$2\Theta_{max}$	50	45
Scan mode	$\omega/2\Theta$	$\omega/2\Theta$
Scan width	1.1	0.95
Standards (hkl)	020, −1 −1 2	021, −3 −1 2, −4 0 0
% mean decay	16	18
No. of measured reflections	1022	2423
No. of unique reflections	425	1882
Reflections in refinement	312 [$\|F_0\| > 2\sigma(F_0)$]	1206 [$\|F_0\| > 6\sigma(F_0)$]
No. of least-squares parameters	19	155
Linear absorption coeff. μ/mm^{-1}	5.56	3.95
Crystal size/mm	0.12 × 0.14 × 0.28	0.15 × 0.18 × 0.20
Range of relative transmission	0.66 − 0.35[e]	0.72 − 0.76
Extinction correction parameter χ[f]	0.034(11)	0.00041(8)
Weights in refinement	$[\sigma^2(F) + 0.0036 F_0^2]^{-1}$	$[\sigma^2(F) + 0.0004 F_0^2]^{-1}$
Largest Δ/σ in final cycle	0.007	< 0.001
$\Delta\varrho_{max}$/(e Å^{-3})	1.48	0.58
$\Delta\varrho_{min}$/(e Å^{-3})	−0.86	−0.45
R[g]	0.063	0.022
wR[h]	0.095	0.027
Goodness of fit	1.18	1.14

[a] Origin choice 2 [27b]. [b] Cell choice 2 [27b]. [c] $a = b = 9.0163 \pm 2$, $c = 11.6078 \pm 4$ Å [24]. [d] Four and six deviating reflections with $\| F_0 \| - \| F_c \| > 6\sigma(F_0)$ omitted from the strontium and barium data, respectively. [e] Absorption correction not applied. [f] $F^* = F[1 + 0.002\chi F^2/\sin 2\Theta]^{-1/4}$. [g] $R = \sum \| F_0 \| - \| F_c \| / \sum |F_0|$. [h] $wR = [\sum w \| F_0 \| - \| F_c \|^2 / \sum w |F_0|^2]^{1/2}$.

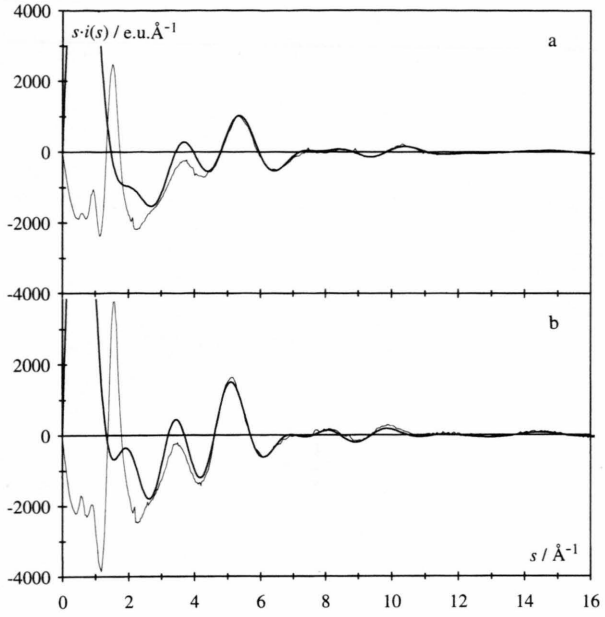

Fig. 1. Reduced LAXS intensity functions, $si(s)$, for the dimethyl sulfoxide solutions of (a) 1.30 M $Sr(CF_3SO_3)_2$ and (b) 1.30 M $Ba(CF_3SO_3)_2$. The experimental and calculated functions are shown with thin and thick lines, respectively.

obtained by a Fourier transformation of the modified intensity function [14] are given in Figure 2.

For the models of the solvated metal ions, the trifluoromethanesulfonate anion, and the solvent molecules, theoretical intensity values were calculated for atomic pair interactions according to (2). Least-squares refinements of the model parameters were carried out by using the STEPLR program [29] to minimize the expression

$$U = \sum s^2 [i_{exp}(s) - i_c(s)]^2. \quad (3)$$

The model fittings were made for data in high s-regions where the diffuse and long-range intensity contributions can be neglected [12b]. Prior to the refinements a Fourier back-transformation procedure was used to correct the $i_{exp}(s)$ functions by removing spurious non-physical peaks below 1.5 Å in the RDFs, which could not be related to intramolecular distances within the solvent molecules or the anions. Model peak shapes were obtained by a Fourier transform of the calculated intensity functions, $i_c(s)$ [14]. A correction for angle-dependent absorption effects [30] was applied for the solutions with linear absorption coefficients lower than 15 cm^{-1}, see Table 1.

EXAFS Data

Sr K edge and Ba L_{III} edge X-ray absorption data were collected in transmission mode at ambient temperature at the Synchrotron Radiation Source (SRS), Daresbury Laboratory, under dedicated conditions, 2.0 GeV and 100 to 200 mA. The wiggler station 9.2 was used for the strontium samples and the bending magnet station 7.1 for barium. The stations were equipped with Si(200) and Si(111) double monochromators, respectively, which during each scan of the absorption range were detuned to less than 50% of the maximum intensity in order to reduce higher order harmonics. The hydrated barium ion samples were also measured at the Stanford Synchrotron Radiation Laboratory (SSRL) using the wiggler beamline 4–1 (Si(111), 3 GeV, ca. 100 mA). The barium solutions were kept in cells with Teflon spacers and Mylar film windows, and the strontium solutions in cells with Vitone spacers and thin (< 40 μm) glass windows. The spacer thickness was varied between 0.5 and 5 mm in order to obtain an absorption change over the edge of about one logarithmic unit. The solid calibration compounds $Ba(H_2O)_8(OH)_2$ and $Sr(H_2O)_8(OH)_2$ were diluted with boron nitride (BN) for the same reason. All spectra were obtained as an average of 3 to 5 scans.

Energy calibration of all spectra was performed using the internal calibration procedure assigning the strontium K edge inflection point of a simultaneously measured solid $Sr(H_2O)_8(OH)_2$ sample to 16108 eV, and likewise, the barium L_{III} edge inflection point of solid $Ba(H_2O)_8(OH)_2$ to 5222 eV. The spectra were processed with the EXAFSPAK program system [31] using standard procedures for pre-edge subtraction and spline removal of the background, and for Fourier filtering [13c]. In the curve-fitting procedures transferability of the phase shift and amplitude parameters for a specific element between compounds of similar structure was assumed. The M–O distances from the solid octahydrates were used for calibration purposes and also the M–O and M–N interactions were modelled using theoretical scattering parameters obtained by means of the FEFF program [17].

Results and Discussion

The Crystal Structure of $Sr(H_2O)_8(OH)_2$

The previous structure description, which was based on film data [18], was confirmed by the present

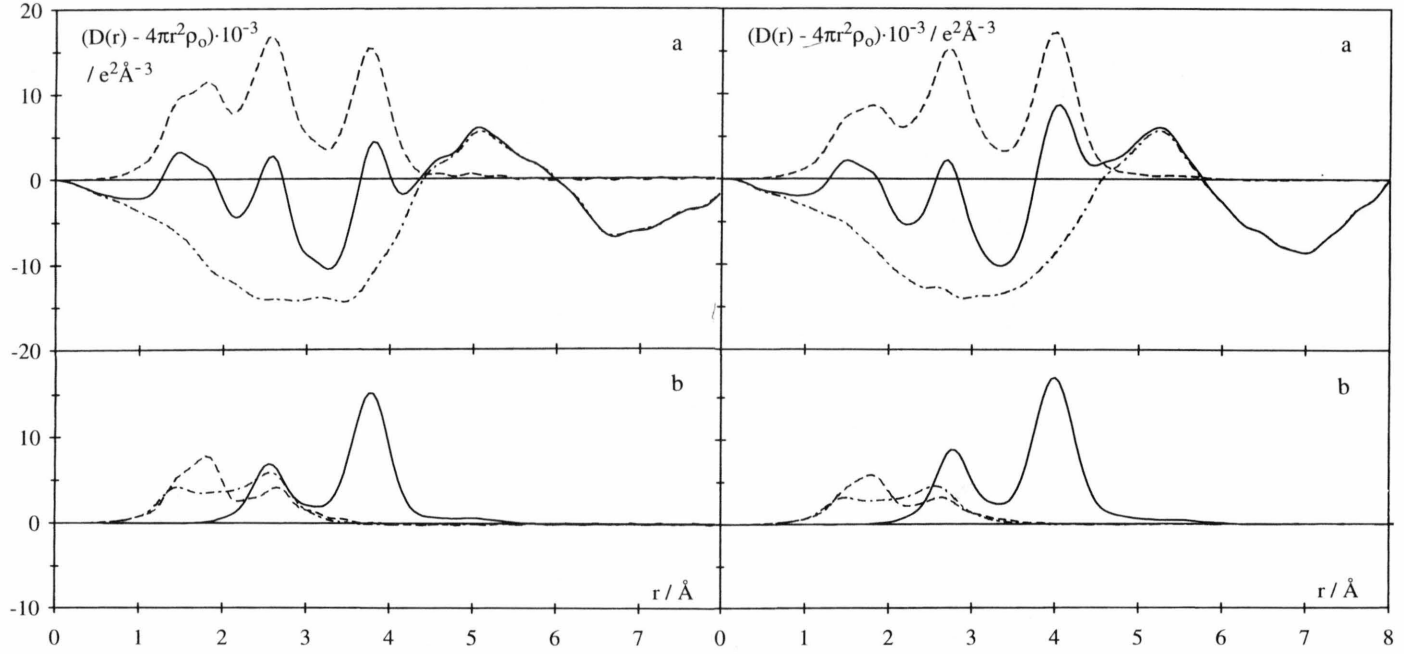

Fig. 2. (a) Experimental radial distribution functions, $D(r) - 4\pi r^2 \varrho_0$ (solid line); sum of calculated peak shapes for molecular models (dashed), and the difference (dash-dotted), for the solutions 1.30 M $Sr(CF_3SO_3)_2$ (left side) and 1.30 M $Ba(CF_3SO_3)_2$ (right side) in dimethyl sulfoxide. (b) Calculated peak shapes for M–O and M···S interactions with parameters according to Table 9 (solid line); Me_2SO (dashed line), and $CF_3SO_3^-$ (dash-dotted line).

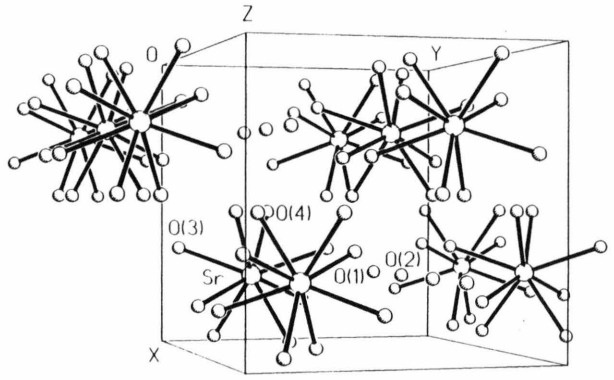

Fig. 3. Crystal structure of $Sr(H_2O)_8(OH)_2$. Unit cell and packing view.

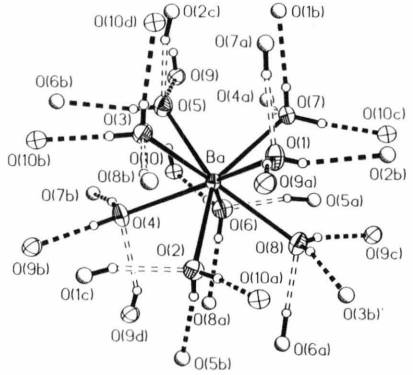

Fig. 4. The hydrogen bonding around the $Ba(H_2O)_8^{2+}$ complex with the 2nd sphere water oxygen atoms represented by shaded circles and the hydroxide ions by ellipsoids. The lone-pair hydrogen bonds from the 1st sphere water oxygen atoms (shaded

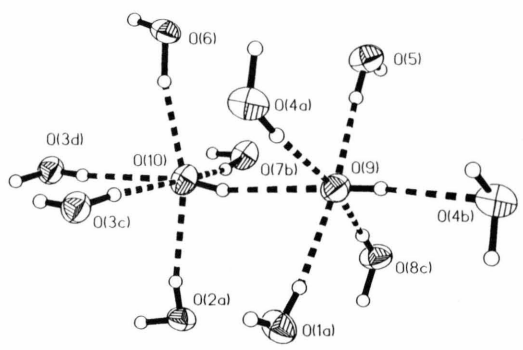

Fig. 5. Hydrogen bonding around the pair of hydroxide ions O(9) and O(10) in the $Ba(H_2O)_8(OH)_2$ structure.

Table 3. $Sr(H_2O)_8(OH)_2$. Fractional atomic coordinates and equivalent isotropic displacement coefficients ($Å^2$) with estimated standard deviations in parenthesis.

Atom	*x/a*	*y/b*	*z/c*	U_{eq} [a]
Sr	0.75	0.25	0.25	0.014(1)
O(1)	0.75	0.75	0.0942(13)	0.017(3)
O(2)	0.75	0.75	0.3409(13)	0.031(4)
O(3)	0.6566(6)	0.0273(6)	0.1257(4)	0.010(1)
O(4)	0.5289(10)	0.3462(9)	0.1233(7)	0.050(2)

[a] Defined as 1/3 of the trace of the orthogonalized U_{ij} tensor.

results. The atomic parameters were transformed to the present setting for the space group *P4/ncc* [27b] and used as starting values for the least squares refinements. The final results are given in Table 3. In addition to the general reflection conditions for this space group the special positions occupied by the strontium atom and the hydroxide oxygen atoms O(1) and O(2) correspond to the special reflection conditions $h + k$, $l = 2n$ and $l = 2n$, respectively [27b]. As previously discussed [18], the positions of the water oxygen atoms O(3) and O(4) almost conform to a C-centering of the tetragonal cell, which explains the observation that almost all reflections with $h + k \neq 2n$ are absent or very weak (except for $l = 4n$). The only observed reflections with odd l values are found for $h, k = 2n$. It was found that the inclusion of the weak reflections in the refinements was important particularly for the determination of the positions of the water oxygen atoms. Even though a higher $\sigma(F_0)$ limit for inclusion of F_0 values in the refinements (Table 2) reduced the R values, the standard deviations of the O(3) and O(4) parameters and the difference between the two Sr–O bond lengths increased. Systematic errors in the intensity data were also evident from the temperature factors of these atoms which could not be made anisotropic for O(3) and yielded a large value for O(4). The shape of the relatively long crystal was not ideal for absorption corrections (Table 2), and the application of a ψ-scan correction did not significantly reduce the standard deviations, nor the R-values. The interatomic distances obtained (Table 4) are however, of sufficient accuracy for the intended comparisons with the solution data, and the similarity with the precisely determined $Ba(H_2O)_8(OH)_2$ structure also allows discussion of the hydrogen bonding (Tables 4 and 5).

The strontium atoms are surrounded by eight water oxygen atoms which form a slightly distorted antiprism (Figure 3). Bond lengths and angles (Table 5) show the hydroxide oxygen atoms O(1) and O(2) to be hydrogen bonded to each other in continuous linear chains running parallel to the c axis, and to four water molecules (Table 5). Each of the two crystallographically different water oxygen atoms O(3) and O(4) forms hydrogen bonds to one of the hydroxide ions and to a water molecule in an adjacent antiprismatic $Sr(H_2O)_8^{2+}$ unit, and accepts a hydrogen bond from another water molecule. A distorted tetrahedral coordination is completed by the bond to the strontium ion (Table 4). The mean Sr–O bond length obtained, 2.62 Å, is somewhat shorter than the mean 2.65 Å in an $Sr–O_8$ polyhedron found in the $Sr(OH)_2 \cdot H_2O$ structure [32] where the trigonal prism of hydroxide ions around the strontium ion is bicapped by the water oxygen atoms.

The Crystal Structure of $Ba(H_2O)_8(OH)_2$

With starting prameters for the barium and oxygen atom positions in the space group $P2_1/n$ obtained by direct methods, full matrix least-squares refinements were carried out. The hydrogen atom positions could be located from Fourier difference syntheses and were refined with a fixed U value of 0.04 $Å^2$. The final residual indices were $R = 0.022$ ($wR = 0.027$) with all non-hydrogen atoms anisotropic. Other details of the refinement conditions can be found in Table 2, and the final structural parameters are given in Table 6 with bond lengths and angles in Tables 7 and 8. The structure can be described as a somewhat irregular Archimedean antiprismatic $Ba(H_2O)_8^{2+}$ unit hydrogen bonded to other units and to the two hydroxide ions [19, 20] (Figure 4). The barium-oxygen distances range from 2.738(4) to 2.824(4) Å, with a mean value of 2.785 Å. A correction for thermal motion assuming the oxygen atoms to ride on the barium atom gave only a slight increase in the mean value to 2.790 Å (Table 7). The O–H distances obtained are, as is normal in X-ray diffraction studies [33a], short with a mean of 0.80 Å and with large standard deviations (0.07 Å).

The previous refinement of the structure gave slightly higher R values, although the reported estimated standard deviations are much smaller, often by a factor 3 or 4 (cf. Table 2 [20]). The present parameter values deviate in several cases more than 3σ from those previously reported, even when using the present standard deviations in Table 6. Especially the positions of two of the hydrogen atoms, H(2A) and H(5A),

Table 4. Strontium-oxygen coordination in $Sr(H_2O)_8(OH)_2$. The Sr–O bond lengths, the hydrogen bonded $O^I \cdots O^{II}$ distances, the $Sr–O^I \cdots O^{II}$ angle β (in degrees) and the $Sr \cdots O^{II}$ distances are given with estimated standard deviations within parenthesis. The first column denotes the type of the hydrogen bonded second shell atom O^{II}: $W = H_2O$, $OH = OH^-$. The lone-pair (LP) bonding of the water molecules O(4)[c] and O(3)[e] has been inferred from comparisons with the $Ba(H_2O)_8(OH)_2$ structure (see text).

O^{II}	$Sr–O^I \cdots O^{II}$	$Sr–O^I$/Å	$O^I \cdots O^{II}$/Å	β	$Sr \cdots O^{II}$/Å
OH	Sr–O(3)···O(1)[a]	2.613(5)	2.665(6)	134.1(3)	4.857(5)
W	Sr–O(3)···O(4)[b]		2.892(9)	123.5(3)	4.848(8)
W(LP)	Sr–O(3)···O(4)[c]		2.847(10)	117.3(2)	4.663(8)
OH	Sr–O(4)···O(2)[d]	2.625(8)	2.692(9)	121.1(4)	4.630(3)
W(LP)	Sr–O(4)···O(3)[e]		2.847(10)	117.0(3)	4.667(5)
W	Sr–O(4)···O(3)[f]		2.892(9)	124.1(3)	4.874(5)
	Mean:	2.619	2.806	122.8	4.757

Symmetry codes: [a] $x, 1+y, z$; [b] $3/2-y, x, z$; [c] $1/2+y, 1-x, -z$; [d] $1-x, 1-y, 1/2-z$; [e] $1/2-y, x, z$; [f] $1/2+y, 1-x, -z$.

Table 5. $Sr(H_2O)_8(OH)_2$ structure. Hydrogen bonds around the hydroxide ions O(1) and O(2) with distances in Å and angles in degrees.

Interaction[b]	Distance	Interaction	Angle
O(1)–O(2)	2.863(21)	O(2)–O(1)–O(3)[a,b,c,d]	82.1(3)
O(1)–O(2)[e]	2.941(21)	O(2)[e]–O(1)–O(3)[a,b,c,d]	97.9(3)
O(1)–O(3)[a,b,c,d]	2.665(6)	O(3)[a,b]–O(1)–O(3)[c,d]	88.9(1)
		O(2)–O(1)–O(2)[e]	180.0(0)
		O(3)[a,c]–O(1)–O(3)[b,d]	164.3(7)
O(2)–O(1)	2.863(21)	O(1)–O(2)–O(4)[f,g,h,i]	98.9(4)
O(2)–O(1)[j]	2.941(21)	O(1)[j]–O(2)–O(4)[f,g,h,i]	81.1(4)
O(2)–O(4)[f,g,h,i]	2.692(9)	O(4)[f,g]–O(2)–O(4)[h,i]	88.6(1)
		O(1)–O(2)–O(1)[j]	180.0(0)
		O(4)[f,h]–O(2)–O(4)[g,i]	162.2(7)

Symmetry code: [a] $x, 1+y, z$; [b] $3/2-x, 1/2-y, z$; [c] $1/2-y, x, z$; [d] $1+y, 3/2-x, z$; [e] $x, y, z-1/2$; [f] $1-x, 1/2+y, 1/2-z$; [g] $1/2+x, 1-y, 1/2-z$; [h] $1/2+y, 1/2+x, 1/2-x$; [i] $1-y, 1-x, 1/2-z$; [j] $x, y, 1/2+z$.

Table 6. $Ba(H_2O)_8(OH)_2$ structure. Fractional atomic coordinates and equivalent isotropic displacement coefficients ($Å^2$)[a] with estimated standard deviations in parenthesis.

Atom	x/a	y/b	z/c	U_{eq}
Ba	−0.00045(4)	0.14811(2)	0.25432(2)	0.0173(1)
O(1)	−0.2122(6)	0.0480(5)	0.3737(3)	0.031(1)
O(2)	−0.2545(5)	0.2478(4)	0.1164(3)	0.026(1)
O(3)	−0.0676(5)	0.3751(4)	0.3959(3)	0.028(1)
O(4)	0.0844(5)	0.3868(5)	0.1461(3)	0.030(1)
O(5)	0.2566(5)	0.2498(5)	0.3794(3)	0.031(1)
O(6)	0.2006(4)	0.0534(5)	0.1169(3)	0.029(1)
O(7)	0.1192(5)	−0.0831(4)	0.3868(3)	0.029(1)
O(8)	−0.1240(5)	−0.0836(5)	0.1261(3)	0.031(1)
O(9)	0.5260(4)	0.1521(4)	0.3925(4)	0.027(1)
O(10)	0.4798(4)	0.1435(4)	0.1398(3)	0.028(1)
H(1A)	−0.221(8)	−0.027(7)	0.361(5)	
H(1B)	−0.286(8)	0.091(8)	0.380(5)	
H(2A)	−0.251(7)	0.238(7)	0.047(5)	
H(2B)	−0.327(8)	0.200(8)	0.120(5)	
H(3A)	−0.034(7)	0.457(3)	0.382(5)	
H(3B)	−0.049(7)	0.374(7)	0.459(5)	
H(4A)	0.184(7)	0.395(7)	0.151(4)	
H(4B)	0.044(7)	0.471(7)	0.135(5)	
H(5A)	0.257(9)	0.337(7)	0.372(5)	
H(5B)	0.338(8)	0.228(8)	0.379(5)	
H(6A)	0.160(7)	0.067(7)	0.049(4)	
H(6B)	0.294(7)	0.077(8)	0.115(5)	
H(7A)	0.134(6)	−0.075(7)	0.453(4)	
H(7B)	0.073(8)	−0.175(8)	0.377(5)	
H(8A)	−0.213(7)	−0.089(8)	0.137(5)	
H(8B)	−0.089(9)	−0.152(8)	0.129(6)	
H(9)	0.532(7)	0.168(7)	0.457(5)	
H(10)	0.505(7)	0.163(7)	0.200(6)	

[a] Defined as 1/3 of the trace of the orthogonalized U_{ij} tensor (a constant value of 0.04 $Å^2$ was used for all hydrogen atoms).

which correspond to Hw(51) and Hw(42) in [20], respectively, differ. The mean value obtained of the Ba–O distances was 2.779 Å, without corrections for thermal motion. The difference from the mean value in the present study corresponds to the smaller values (by 0.3%) reported of the unit cell edges, which were determined from 25 centered reflections in the low-angle range $6 < \theta < 13°$ [20]. The variation of the results provides yet another example "that the precision with which parameters can be determined on a diffractometer may conceal a serious lack of accuracy" [34].

The hydrogen bonding in the structure is evident from the relatively short O···O distances (2.64 to 2.99 Å), see Tables 7 and 8. A unique hydrogen bond arrangement is found around the two hydroxide ions, with five hydrogen bonds accepted and one donated forming fairly regular oxygen atom octahedra around the central hydroxide oxygen atom, Table 8. One hydroxide ion, O(10), donates its proton to the other, O(9), which in its turn donates its proton to a water molecule coordinated to barium. Figure 5. In other

Table 7. Barium-oxygen coordination in the $Ba(H_2O)_8(OH)_2$ structure. The Ba–O^I bond lengths, hydrogen bonded $O^I \cdots O^{II}$ distances, $Ba \cdots O^{II}$ distances and the Ba–$O^I \cdots O^{II}$ angle β (in degrees) are given with estimated standard deviations within parenthesis. The Ba–O^I distances within the square brackets are corrected for thermal motion assuming oxygen to ride on the barium atom. The different types of the hydrogen-bonded 2nd shell O^{II} atoms are denoted: W = H_2O, OH = OH^-, and LP which signifies bonded via the lone-pair of the O^I oxygen atom.

O^{II}	Ba–$O^I \cdots O^{II}$	Ba–O^I/Å	$O^I \cdots O^{II}$/Å	β	$Ba \cdots O^{II}$/Å
W	Ba–O(1)···O(2)[a]	2.758(5) [2.764]	2.881(6)	116.6(2)	4.739(5)
OH	Ba–O(1)···O(9)[b]		2.662(7)	131.0(2)	4.932(4)
W, LP	Ba–O(1)···O(7)[c]		2.854(5)	109.9(2)	4.596(4)
W	Ba–O(2)···O(5)[d]	2.813(4) [2.815]	2.826(6)	115.0(2)	4.755(4)
OH	Ba–O(2)···O(10)[b]		2.708(6)	121.4(2)	4.814(4)
W, LP	Ba–O(2)···O(1)[e]		2.811(6)	113.0(2)	4.688(5)
OH	Ba–O(3)···O(10)[f]	2.824(5) [2.828]	2.678(6)	120.0(2)	4.766(4)
OH	Ba–O(3)···O(10)[g]		2.859(5)	122.8(2)	4.990(4)
W, LP	Ba–O(3)···O(8)[e]		2.865(7)	110.9(2)	4.685(5)
W	Ba–O(4)···O(7)[f]	2.738(4) [2.744]	2.857(7)	119.9(2)	4.842(5)
OH	Ba–O(4)···O(9)[f]		2.681(6)	113.9(2)	4.987(4)
OH, LP	Ba–O(4)···O(9)[h]		2.991(5)	110.6(2)	4.712(4)
W	Ba–O(5)···O(6)[f]	2.776(5) [2.781]	2.848(7)	116.9(2)	4.791(5)
OH	Ba–O(5)···O(9)		2.647(6)	130.1(2)	4.916(4)
W, LP	Ba–O(5)···O(2)[i]		2.826(6)	111.8(2)	4.639(4)
W	Ba–O(6)···O(8)[j]	2.806(4) [2.810]	2.870(5)	117.9(2)	4.862(5)
OH	Ba–O(6)···O(10)		2.702(6)	124.2(2)	4.866(5)
W, LP	Ba–O(6)···O(5)[h]		2.848(7)	113.9(2)	4.740(5)
W	Ba–O(7)···O(1)[l]	2.788(4) [2.793]	2.854(5)	120.3(2)	4.894(4)
OH	Ba–O(7)···O(10)[k]		2.703(6)	124.0(2)	4.848(4)
W, LP	Ba–O(7)···O(4)[k]		2.857(7)	107.9(2)	4.565(5)
W	Ba–O(8)···O(3)[a]	2.779(4) [2.784]	2.865(7)	118.5(2)	4.850(4)
OH	Ba–O(8)···O(9)[k]		2.641(6)	130.3(2)	4.918(4)
W, LP	Ba–O(8)···O(6)[j]		2.870(5)	119.3(2)	4.875(4)
	Mean:	2.785 [2.790]	2.797	119.2	4.803

Symmetry codes: [a] $-\frac{1}{2}-x, y-\frac{1}{2}, \frac{1}{2}-z$; [b] $x-1, y, z$; [c] $-x, -y, 1-z$; [d] $x-\frac{1}{2}, \frac{1}{2}-y, z-\frac{1}{2}$; [e] $-\frac{1}{2}-x, \frac{1}{2}+y, \frac{1}{2}-z$; [f] $\frac{1}{2}-x, \frac{1}{2}+y, \frac{1}{2}-z$; [g] $x-\frac{1}{2}, \frac{1}{2}-y, \frac{1}{2}+z$; [h] $x-\frac{1}{2}, \frac{1}{2}-y, z-\frac{1}{2}$; [i] $x+\frac{1}{2}, \frac{1}{2}-y, \frac{1}{2}+z$; [j] $-x, -y, -z$; [k] $\frac{1}{2}-x, y-\frac{1}{2}, \frac{1}{2}-z$; [l] $-x, -y, 1-z$.

Table 8. $Ba(H_2O)_8(OH)_2$ structure. Hydrogen bonded O···O distances (in Å) around the hydroxide ions O(9) and O(10) with estimated standard deviations within parenthesis.

Interaction	Distance	Interaction	Distance
O(9)···O(1)[a]	2.661(7)	O(10)···O(2)[a]	2.708(6)
O(9)···O(4)[b]	2.681(6)	O(10)···O(3)[b]	2.678(6)
O(9)···O(4)[c]	2.991(5)	O(10)···O(3)[d]	2.859(5)
O(9)···O(5)	2.646(6)	O(10)···O(6)	2.702(6)
O(9)···O(8)[e]	2.640(6)	O(10)···O(7)[e]	2.703(6)
O(9)···O(10)	2.960(5)		

Symmetry codes: [a] $1+x, y, z$; [b] $\frac{1}{2}-x, y-\frac{1}{2}, \frac{1}{2}-z$; [c] $\frac{1}{2}+x, \frac{1}{2}-y, z-\frac{1}{2}$; [d] $\frac{1}{2}+x, \frac{1}{2}-y, \frac{1}{2}+z$; [e] $\frac{1}{2}-x, \frac{1}{2}+y, \frac{1}{2}-z$.

investigated hydrated barium hydroxides, in which the hydroxide ions serve as ligands, the hydroxide protons do not form hydrogen bonds [32, 35]. However, as pointed out by Lutz, a metal ion-oxygen interaction seems to strengthen the O–H bond of a hydroxide ligand and thus reduce its hydrogen bond donor ability, contrary to the effect on coordinated water molecules [36]. This is consistent with the present observations that the proton of the non-coordinated hydroxide ions is involved in hydrogen bonding.

All 18 hydrogen atoms of the $Ba(H_2O)_8(OH)_2$ compound are involved in a network of slightly bent and asymmetrical hydrogen bonds, the strongest of which are those donated from the water molecules to the hydroxide ions. All water oxygen atoms accept one hydrogen bond (from water molecules except in one case, Table 7) and donate two hydrogen bonds to water or hydroxide oxygen atoms (Figure 4). The bond to the barium ion completes a distorted tetrahedral coordination around all water oxygen atoms, in which generally the $Ba–O_I \cdots O_{II}$ angles are larger than tetrahedral (mean 119.2°) with the largest angles for hydro-

gen bonds donated to the hydroxide oxygen atoms (mean 126.4°) and the smallest to oxygen atoms hydrogen bonded *via* the lone-pair (mean 112.2°). These observations have been used to identify the probable lone-pair hydrogen bonds to the oxygen atoms of the $Sr(H_2O)_8^{2+}$ unit in the $Sr(H_2O)_8(OH)_2$ structure (Table 4). The hydrogen bonded pairs of hydroxide ions in the $Ba(H_2O)_8(OH)_2$ structure is a unique feature, and constitutes the most striking difference from the more regular bonding arrangement in the $Sr(H_2O)_8(OH)_2$ crystal structure where the hydroxide ions form linear chains.

Previously, a distorted antiprismatic 8-coordination of water oxygen atoms and hydroxide ions around a barium ion has also been found in the trihydrate $Ba(OH)_2 \cdot 3H_2O$ with a mean Ba–O distance of 2.813 Å [32, 35]. A longer mean distance, 2.855 Å, is found in the $Ba-O_8$ polyhedron of β-$Ba(OH)_2 \cdot H_2O$ [32], which is isostructural with the $Sr(OH)_2 \cdot H_2O$ compound mentioned above. The increase in the Ba–O distance is probably mainly a result of the increasing number of bridging oxygen atoms shared between the barium atoms in the structures. In the corner- and edge-sharing $Ba-O_9$ polyhedra (tricapped trigonal prism) in γ-$Ba(OH)_2 \cdot H_2O$ the mean Ba–O distance is even longer, 2.886 Å [32] and increases to 2.987 Å in the near-icosahedral $Ba-O_{12}$ polyhedron in $Ba(BrO_4)_2 \cdot 3H_2O$ [37]. The water molecules in all the hydrated hydroxides are involved in strong hydrogen bonding, particularly to the hydroxo ligands which are strong proton acceptors [36]. The Ba–O distances to water molecules are on the average 0.12 Å longer than to coordinated hydroxide oxygen atoms in these compounds [32]. In $Ba[Co(NCS)_4] \cdot 7H_2O$ the mean Ba–O distance of the $BaS(H_2O)_9$ polyhedron is 2.91 Å, although the mean value to the five non-bridging water molecules is 2.80 Å, close to that in the present study [38].

Thus, the most important factors decreasing the Ba–O coordination distances seem to be 1. a decrease in coordination number, 2. if the oxygen atom belongs to a hydroxide ion instead of a water molecule, 3. if it is non-bridging, or 4. strongly hydrogen bonded.

An interesting observation with implications for the solution structure is the second shell consisting of 24 hydrogen-bonded oxygen atoms which can be distinguished around both the strontium and barium ions in the $M(H_2O)_8(OH)_2$ crystals (Figure 4). The average $Sr \cdots O^{II}$ distance is 4.76 Å (range 4.63 to 4.87 Å, Table 4) and the $Ba \cdots O^{II}$ 4.80 Å (range 4.56 to 4.99 Å, Table 7), with a broader distribution in the less symmetrical structure of the $Ba(H_2O)_8(OH)_2$ compound. Even though the difference between the mean $M-O^I$ distances is 0.17 Å for M = Ba and Sr, the corresponding $M \cdots O^{II}$ difference is only 0.05 Å probably due to the steric requirements to accommodate the 24 oxygen atoms.

The mean hydrogen bonded $O^I \cdots O^{II}$ distance is 2.80 Å in the barium structure (2.85 Å between water oxygen atoms only, see Table 7). The corresponding $O^I \cdots O^{II}$ distance between hydrogen-bonded water molecules around Ba^{2+} in aqueous solution is found to have a broad distribution around 2.89 Å [39]. The hydrogen bonds are weaker than those found in the same way for bulk water ($O \cdots O$ 2.86 Å) [39] and around smaller divalent cations (e.g. Mn^{2+} and Ni^{2+}, $O^I \cdots O^{II}$: 2.76 Å) [39, 40], but comparable to those around Ca^{2+} [41, 42]. The distances given above have been derived from OD stretching frequencies measured by infrared spectroscopic methods of isotopically dilute HDO molecules coordinated to the ions in aqueous solution, by means of a correlation with OD frequency values obtained for precisely determined crystal structures [43].

Evaluation of the LAXS Measurements

The radial distribution functions for the dimethyl sulfoxide solutions of the trifluoromethanesulfonate salts (Fig. 2), show two distinct peaks at 2.55 and 3.8 Å for strontium, and at 2.75 and 4.0 Å for barium, corresponding to the M–O and M–S distances with the solvated ions, respectively. The broad and diffuse peaks in the region 1.5 to 2.7 Å correspond to intramolecular distances in the dimethyl sulfoxide molecules [44] and in the trifluoromethanesulfonate ions [45]. The large and broad peaks at about 5.5 Å are always found in dimethyl sulfoxide solutions and originate from the bulk solvent structure [44, 46].

Least-squares refinements have been performed of the parameters describing the M–O and $M \cdots S$ interactions according to (2) and (3), and the results are summarized in Table 9. Due to the strong correlation between the parameter l of the Debye-Waller factor, $\exp(-\frac{1}{2} l^2 s^2)$, and the frequency n of the corresponding interatomic interactions, the model fitting was performed by varying the distance d and the l parameters for fixed values of $n = 4, 5, 6, 8$, and 10. The lowest error square sum was obtained with $n = 6$ for both metal ions. The consistency of the best set of parame-

Table 9. LAXS results. The parameters[a] are the frequency n of the interatomic distances d, and their root-mean-square variations l.

Ion	Solvent	Interaction	d/Å	l/Å	n
Sr^{2+}	Water	$Sr-O^{I}$	2.64(2)	0.13(2)	8.1(3)
		$Sr\cdots O^{II}_{hyd}$ [b]	4.78(5)	0.35	13.3(10)
		$Sr-O^{II}_{int}$ [c]	4.10(10)	0.20(5)	2.5(5)
		$Sr\cdots H^{I}$ [d]	3.25	0.24	16.2
		$Sr\cdots H^{II}$ [d]	5.3	0.35	26.6
Ba^{2+}	Water	$Ba-O^{I}$	2.82(2)	0.13(2)	8.1(3)
		$Ba\cdots O^{II}_{hyd}$ [b]	4.90(5)	0.35	13.3(10)
		$Ba\cdots O^{II}_{int}$ [c]	4.15(10)	0.20(5)	2.5(5)
		$Ba\cdots H^{I}$ [d]	3.40	0.24	16.2
		$Ba\cdots H^{II}$ [d]	5.4	0.35	26.6
Sr^{2+}	Me_2SO	S–O	2.54(1)	0.11(1)	6
		$Sr\cdots S$	3.77(1)	0.16(1)	6
Ba^{2+}	Me_2SO	Ba–O	2.76(1)	0.15(1)	6
		$Ba\cdots S$	3.99(1)	0.22(1)	6

[a] For the refined parameters estimated standard deviations are given within brackets. [b] Second sphere hydrogen-bonded water oxygen atom. [c] Non-hydrogen bonded water oxygen atom between first sphere aqua ligands. [d] Assumed hydrogen atom positions for 1st and 2nd sphere oxygen atoms, O^{I} and O^{II}, respectively.

ters was checked by varying the s region (especially its lower limit) for the refinements.

The RDFs of the aqueous 0.82 M $Sr(ClO_4)_2$ and $Ba(ClO_4)_2$ solutions are not equally straightforward to interpret as for the dimethyl sulfoxide solutions. A specially adapted difference procedure had to be employed in order to eliminate the overlap with the hydrogen bonded $O\cdots O$ distances between water molecules in the bulk water and around the ClO_4^- ions [39], thus allowing reliable information to be obtained. In a previous study it was shown that the close structural similarity of the trivalent yttrium and erbium ions in aqueous perchlorate solution can be used for isostructural substitution in order to separate the RDFs into one part comprising only interatomic interactions involving the erbium ions, $\Delta D^{Er}(r)$, and another part with all remaining solvent and anion interactions excluding erbium [12]. The latter RDF part (curve c for ClO4A in Fig. 5 of [12a]), which contains not only intramolecular ClO_4^- and H_2O distances but also H_2O–H_2O and ClO_4^-–H_2O interactions in the bulk water and in the vicinity of the Er^{3+} and ClO_4^- ions, was subtracted from the total RDFs of the strontium and barium perchlorate solutions after proper scaling. Corrections were made to account for the concentration and structural differences in the solutions affecting the H_2O–H_2O interactions, by including a contribution from the RDF of pure water and by assuming probable configurations of the coordinated water molecules around the metal ions. The resulting difference curves, $\Delta D^{Sr}(r)$ and $\Delta D^{Ba}(r)$ shown in Figure 6, were obtained assuming $H_2O\cdots H_2O$ configurations intermediate to regular antiprismatic and cubic structures around the octahydrated metal ions, and consist essentially of the interatomic interactions involving the metal ions. Hence, the distinct peaks centered at about 2.6 and 2.8 Å originate from the first hydration sphere around the Sr^{2+} and Ba^{2+} ions, respectively. By fitting peak shapes obtained by a Fourier transformation of the calculated intensity contributions, see (2), from assumed Gaussian distributions of the $M-O^{I}$ bond lengths (also including M–H distances), these experimental peaks were found to correspond to 8.1(3) water molecules with $M-O^{I}$ distances of 2.64(2) and 2.82(2) Å for M = Sr and Ba, respectively. The resulting structural parameters are given in Table 9, with the error limits estimated by varying the scaling and correction factors in the procedure used to eliminate the background interactions.

The difference in solvation number between the aqueous and dimethyl sulfoxide solutions is also shown by the difference in $M-O^{I}$ bond length, about 0.09 and 0.05 Å for strontium and barium, which corresponds well to the expected decrease in bond length from 8- to 6-coordination, 0.09 and 0.06 Å, respectively [47]. Previous studies of dimethyl sulfoxide solvates of relatively hard acceptors show that similar M–O bond lengths as in the hydrates would be expected for the same coordination number [48, 49], and the shorter distances in dimethyl sulfoxide solution are thus consistent with the LAXS results indicating six-coordination (Table 9).

The $\Delta D^{Sr}(r)$ and $\Delta D^{Ba}(r)$ functions indicate a somewhat higher probability of finding surrounding water molecules at the distance expected for hydrogen bonding to the first hydration sphere, i.e. at the mean $M\cdots O^{II}$ distance from the crystal structures (Tables 4, 7). This tendency is slightly more pronounced for the strontium ion although there is no sharp limit towards longer distances (Figure 6). Assuming a broad Gaussian distribution of oxygen atoms ($l = 0.35$ Å), calculated model peaks corresponding to 13.3(1.0) water molecules with $M\cdots O^{II}$ distances of 4.78(5) and 4.90(5) Å could be fitted to the $\Delta D^{Sr}(r)$ and $\Delta D^{Ba}(r)$ curves for M = Sr and Ba, respectively. Minor contributions still remain corresponding to 2.5(5) water molecules at 4.10(10) and 4.15(10) Å from the Sr^{2+} and Ba^{2+} ions, respectively. Such dis-

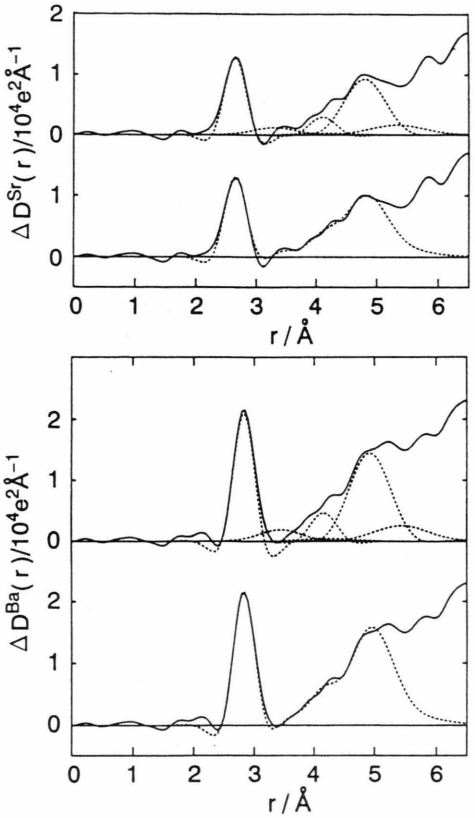

Fig. 6. Difference RDFs (solid lines), $\Delta D^{Sr}(r)$ and $\Delta D^{Ba}(r)$, for aqueous solutions of (a) 0.82 M $Sr(ClO_4)_2$ and (b) 0.82 M $Ba(ClO_4)_2$ (see text). Calculated model peak shapes (dashed lines, parameters according to Table 9) are shown for the individual interatomic interactions with the metal ion (upper part), with the fit of their sum displayed below.

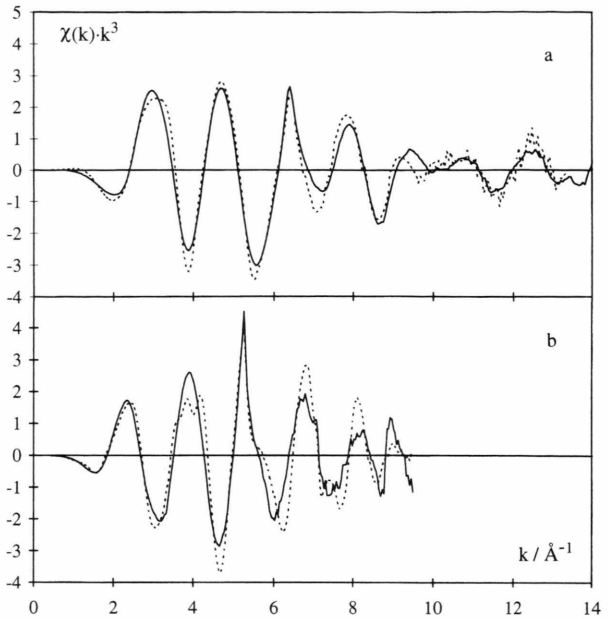

Fig. 7. Comparisons of EXAFS spectra of hydrated (a) strontium and (b) barium ions in aqueous solution (solid line) and in the solid state (dashed line).

tances would give improbable hydrogen bond angles to the aqua ligands of the first hydration sphere and these water molecules must, therefore, occupy interstitial space between these ligands. The fits of the models are shown in Figure 7, including assumed M···H interactions from the water molecules, and account satisfactorily for all interatomic interactions up to a distance of 5 Å around the metal ions.

In the previous investigation the first Er–O peak at 2.35 Å in the $\Delta D^{Er}(r)$ curve corresponding to a hydration number of 8.0(3), was fully resolved from a well-defined M···O^{II} peak centered at 4.5 Å, with almost zero value of the atomic distribution between 3 to 4 Å [12]. The number of second sphere water molecules was estimated to be about 16 from the solution X-ray diffraction data. This is consistent with infrared spectroscopic studies of the O–D stretching vibrations of the water molecules around the trivalent lanthanide ions [40], which show stronger hydrogen bonding to a second hydration shell than that for the Ca^{2+} and Ba^{2+} ions [39, 41].

The picture that emerges for the hydration structure around the large octahydrated Sr^{2+} and Ba^{2+} ions in aqueous solution is a very flexible geometrical arrangement and conformation of the eight first-sphere aqua ligands, loosely hydrogen bonded to surrounding water molecules in the bulk water. Within this diffuse second hydration sphere there are also water molecules not hydrogen-bonded to those in the first-sphere, which can approach the metal ion more closely than the hydrogen-bonded ones.

Interpretation of the EXAFS Measurements

The EXAFS spectra of the hydrated strontium and barium ions in aqueous solution are similar to the corresponding spectra of the eight-coordinated solid hydrates, $Sr(H_2O)_8(OH)_2$ and $Ba(H_2O)_8(OH)_2$, see Figure 7. The metal ion-oxygen peaks in the Fourier transforms (Fig. 8) show, as also the LAXS results, distinct first hydration spheres in solution, with M–O^I distances similar or slightly longer than those

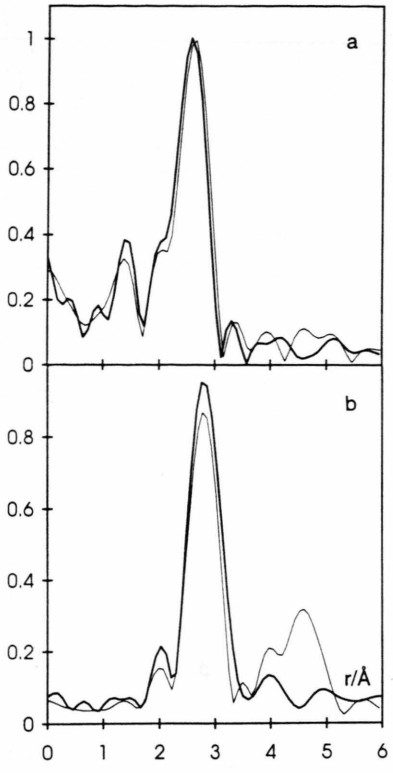

Fig. 8. Fourier transforms of the EXAFS spectra in Fig. 7 for the hydrated ions a) strontium and (b) barium (thick line: solution; thin line: solid).

Table 10. EXAFS results. The refined parameters are: the number n of interatomic distances d, and the parameter $\Delta\sigma^2$ of the Debye-Waller factor[a]. The estimated uncertainty (≈ 2 standard deviations) is given within parenthesis.

Ion	Solvent	Interaction	d/Å	$\sigma^2 \cdot 10^{-3}$/Å^2	n[b]
Sr^{2+}	Water	Sr–O	2.61(1)	11.6(5)	8
Sr^{2+}	Me_2SO	Sr–O	2.54(1)	8.2(4)[c]	6
Sr^{2+}	Pyridine	Sr–N	2.57(2)	11.6(5)	6
Ba^{2+}	Water	Ba–O	2.80(3)[d]	11.2(4)[e]	8
Ba^{2+}	Pyridine	Ba–N	2.78(3)	13.7(5)	6

[a] Absolute value obtained with the use of theoretical FEFF parameters [17]. [b] Fixed value. [c] No significant contribution from Sr–S. [d] Average value of two groups of Ba–4O distances about 0.10 Å apart. [e] Mean value for the two groups of Ba–O distances.

in the solid octahydrates (Table 10). Significant anharmonicity occurs in the distribution of the Ba–O distances both in the solid state and in aqueous solution and is manifested in several ways. Firstly, tailing is observed on the long distance side of the Ba–O peak (Figure 8). Secondly, fitting the EXAFS spectra of the solid $Ba(H_2O)_8(OH)_2$ with a model function for a single Ba–O distance, with the use of theoretical back-scattering parameters calculated *ab initio* by means of the FEFF [17] program, resulted in a significantly shorter value (by about 0.05 Å) than the mean from the crystal structure, 2.79 Å. By assuming two groups of Ba–4O distances in the least-squares refinements (difference about 0.10 Å) close agreement of the mean values is obtained. The aqueous solution shows a similar behaviour with the FEFF parameters, although with a slightly longer mean of the two groups of Ba–O distances (Table 10). However, a single distance adequately explains the EXAFS patterns when model-based back-scattering parameters extracted from the spectra of the solid compounds are used, and also for the presumably (see below) six-coordinated barium ion in pyridine solution, as well as for the solvated strontium ions.

We encountered a curious feature in all our EXAFS spectra which is more emphasized for the samples containing barium ions. It is evident that the features at ca. 6.4 Å^{-1} in the Sr K edge spectra and at ca. 5.3 Å^{-1} in the Ba L_{III} edge EXAFS spectra (Fig. 9) are sharper and of a different shape than what can be modelled by normal curve-fitting. We have ensured that this feature is not instrumental by measuring barium samples using both the SRS and SSRL facilities, with no change. By means of the FEFF program [17] we have checked that there is no multiple scattering path of importance in the $[Sr(OH_2)_8]^{2+}$ and $[Ba(OH_2)_8]^{2+}$ complexes. At present we do not have any plausible explanation of this phenomenon which has an appearance as if caused by an electronic transition. The spline-fitting to obtain the zero level of the EXAFS function [13] becomes very difficult due to this feature. Even if the evaluation of metal ion-ligand distances has not been seriously affected, it has not been possible to fit the EXAFS amplitude reliably enough in order to determine the coordination numbers.

The metal-nitrogen bond distances for the solvated barium and strontium ions in the rather dilute pyridine solutions which only could be determined by means of the EXAFS technique, are similar or shorter than the corresponding metal-oxygen distances, Table 10. However, the nitrogen atom in pyridine and aromatic rings is known to have a somewhat larger radius than the oxygen atom in water. For example, in the distorted cubic eight-coordination around

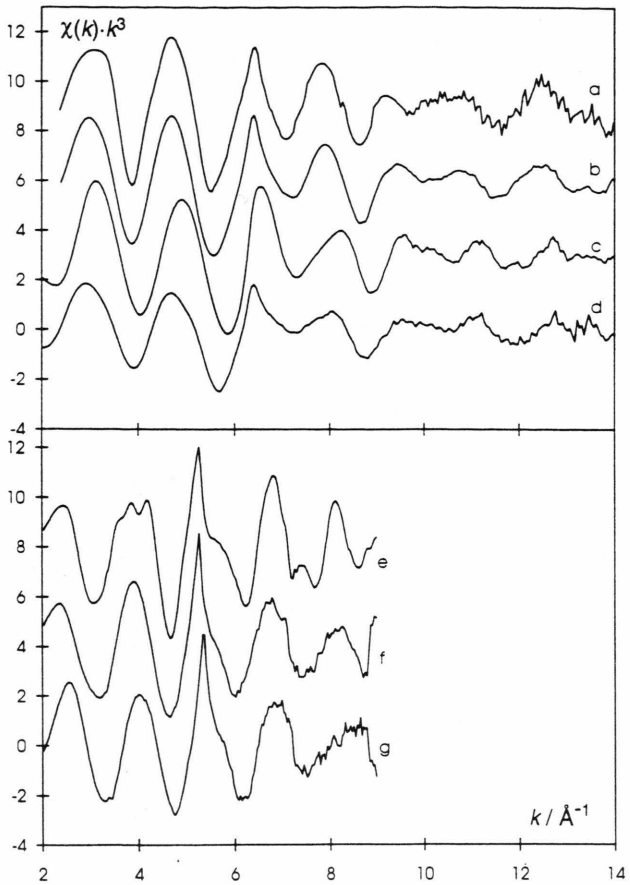

Fig. 9. Unfiltered EXAFS spectra for (a) solid $Sr(H_2O)_8(OH)_2$ (offset +9.0), (b) 0.10 M $Sr(CF_3SO_3)_2$ in water (+6.0), (c) 1.30 M $Sr(CF_3SO_3)_2$ in dimethyl sulfoxide (+3.0), (d) 0.10 M $Sr(CF_3SO_3)_2$ in pyridine, (e) solid $Ba(H_2O)_8(OH_2$ (+6.0), (f) 0.20 M $Ba(CF_3SO_3)_2$ in water (+3.0), (g) 0.10 M $Ba(CF_3SO_3)_2$ in pyridine.

strontium and barium ions in their tetraaquabis(1,10-phenantroline) complexes [50], the mean Sr–N (2.79 Å) and Ba–N (2.96 Å) distances are much longer than those in the present study, 2.57 and 2.78 Å, respectively, and also 0.19 Å longer than the mean Sr–O and Ba–O distances in the same complex, although this difference certainly is enlarged by the rigidity of the bidentate phenantroline ligand. Moreover, the difference in the mean bond lengths between the hexakis-pyridine and hexaaqua complexes of iron(II) is 0.15 Å [51, 52], but is probably enlarged by steric effects for the pyridine ligands around this small ion. A better measure of the size difference seems to be given by the solvated Cu^{2+} ion which is less crowded due to its Jahn-Teller distortion. The mean of the four distances in the equatorial plane is 2.02 Å for $Cu-4NC_5H_5$ [53] and 1.96 Å for $Cu-4OH_2$ [54] in crystal structures.

Consequently, the present results (Table 10) indicate a decrease in the solvation number, probably to six, from water to pyridine. For the hard strontium and barium ions forming metal-ligand bonds with mainly electrostatic character, this must be a result of sterical effects as both the pyridine and dimethyl sulfoxide ligands require more space than a coordinated water molecule.

The Sr L_{III} and Ba K absorption edges show no characteristic features, and no information on the coordination could be obtained from the XANES region of the spectra.

Hydration of the Alkaline-Earth Metal Ions

For the calcium ion in solution there is evidence from a number of different studies, for example comparisons of Ca–O distances in solution [10] with hydrated ions in solids [42] and from theoretical calculations [55], that the average hydration number is greater than six in aqueous solution, with a probable value of about seven. In addition, a comparison of the partial molar hydration volumes V_i^0 (relative to zero for the proton) in the series Be^{2+} −12.0, Mg^{2+} −21.2, Ca^{2+} −17.9, Sr^{2+} −18.2, and Ba^{2+} −12.5 $cm^3\,mol^{-1}$ [56] gives a similar picture. Normally the V_i^0 values are expected to increase monotonously with increasing ionic radii for a group of ions with the same charge, because of the dominating contributions from the increasing intrinsic volume of the ion, and the increase in volume by the reduced electrostriction of the solvent molecules surrounding the ion [57, 58]. If the Ca^{2+} ion has a hydration number of eight as for Sr^{2+} and Ba^{2+}, its V_i^0 value would be expected to be smaller (more negative) than that of Sr^{2+}. On the other hand the increase (3.3 $cm^3\,mol^{-1}$) as compared to the V_i^0 value of the smaller Mg^{2+} ion (cf. the increase 5.7 $cm^3\,mol^{-1}$ from Ba^{2+} to Sr^{2+}), should have been larger assuming the same hydration number of six as for Mg^{2+} [10]. In this qualitative comparison contributions to the relative volume increase are caused not only by the longer $M-O^I$ distances (about 2.42 Å for Ca–O and 2.09 Å for Mg–O) [10, 12b] but also by the weaker hydrogen bonding around the hydrated Ca^{2+} ion; the $O^I\cdots O^{II}$ distances are about 2.89 and 2.76 Å around the hydrated Ca^{2+} and Mg^{2+} ions, respectively [39, 41]. Previously, hydration numbers of seven and eight were also proposed for the

Ca^{2+} and Sr^{2+} ions, respectively, from a more general semi-empirical correlation between V_i^0 and an effective size of the hydrated ions, although with this correlation the very small Be^{2+} ion was found to deviate from the expected value of four [58]. The decrease in hydration number from six to four for the strongly polarizing Be^{2+} ion [10] as compared to Mg^{2+}, is reflected in the strong increase in its partial molar volume, despite the strong electrostriction of the water ligands and the short and strong hydrogen bonds formed around Be^{2+} [59, 60]. Thus, the hydration numbers in aqueous solution of the divalent alkaline earth metal ions decrease from eight for the large Ba^{2+} and Sr^{2+} ions, about seven for Ca^{2+}, six for Mg^{2+}, to four for Be^{2+}. No concentration dependence of the hydration number was detected for the solutions in the present study, cf. Table 1, although it has been pointed out from a survey of crystal structures of hydrated calcium and magnesium ions that at least for the calcium ion in the solid state the coordination number is variable and affected by the hydrogen bonding to the second coordination sphere [42b].

A plot of the single ion hydration enthalpies [61] was found to closely follow a linear correlation versus $1/d$ for the large range of M–O distances d for Be^{2+} to Ba^{2+} (Figure 10). The Be–O distance used $d = 1.67$ Å, from the only experimental LAXS determination in solution [62] gave the best fit to a straight line, although no error limit was given and the deviation from the crystal structure values around 1.62 Å [59] is rather large. For Ra^{2+} the d(Ra–O) distance in eight-coordination was assumed to be 0.06 Å longer than d(Ba–O), based on the difference in their effective ionic radii for this coordination number [47]. Also the value for 12-coordination estimated in a similar way is indicated in the figure.

According to the Born equation the heat change associated with the introduction of the ion into a solvent regarded as a dielectric continuum follows a $1/d$ relation [63], with d proposed to be a cavity radius [64]. For a real hydration process of an ion the bonding of water molecules in the first hydration shell is expected to give a contribution from higher order terms (d^{-2}, d^{-3} and d^{-4} for the interactions ion-dipole, ion-quadrupole and ion-induced dipoles by polarization, etc. [63]). However, there are counteracting contributions for example from ligand-ligand repulsion and dielectric saturation effects [57, 65], and $1/d$ relations have previously been found to be adequate for a description of the variations in theoretical binding

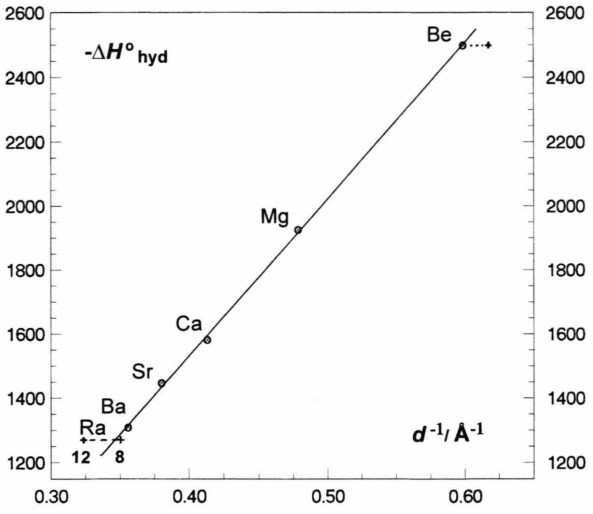

Fig. 10. Hydration enthalpy versus $1/d$(M–O) for the alkaline earth metal ions. The values used for the correlation line are (circles) M^{2+}, $-\Delta H^0_{hyd}$/kJ mol^{-1}, d(M–O)/Å: Be^{2+}, 2494, 1.67; Mg^{2+}, 1921, 2.09; Ca^{2+}, 1577, 2.42; Sr^{2+}, 1443, 2.63; Ba^{2+}, 1305, 2.81. In addition the values Be^{2+}, 2494, 1.62 (from crystal structures); Ra^{2+}, 1266, 2.87 (8-coordination); Ra^{2+}, 1266, 3.09 (12-coordination), are given as crosses (see text).

energies for isolated clusters of the hexahydrated di- and trivalent transition metal ions [66]. Considering the large decrease of the hydration numbers for the alkaline earth metal group of ions, including also the tetrahydrated Be^{2+} ion with a high degree of charge-transfer in the bonds [60], the almost complete compensation of the higher-order d^{-n} terms as indicated by the correlation in Fig. 10, is remarkable. However, the ligand-ligand repulsion must be especially conspicuous in the tetrahedral $Be(H_2O)_4^{2+}$ complex with a mean O–O distance of 2.73 Å for d(Be–O) = 1.67 Å [62]. Also previously, in an attempt to find a more general semi-empirical expression, the hydration enthalpies of the alkaline earth ions were proposed to follow a $1/d$ correlation, but with smaller d values and with Be^{2+} and Ra^{2+} excluded [64]. In the present case the extrapolation of the correlation line to include the hydration enthalpy of Ra^{2+} gives an estimated hydration number of 8.5 ± 0.5 (Figure 10).

Conclusions

A summary of the "best" values obtained for the metal ion-oxygen distances of the solvated strontium

Table 11. Summary of bond distances d and coordination numbers n for the solvated Sr^{2+} and Ba^{2+} ions with estimated standard deviations given in parenthesis.

Solvent or ligand	M–X	d/Å	n	Method
H_2O(solution)	Sr–O	2.63(2)	8	X-ray diffraction, EXAFS
H_2O(solid)	Sr–O	2.62(1)[a]	8	X-ray crystallography
DMSO(solution)	Sr–O	2.54(1)	6	X-ray diffraction, EXAFS
Pyridine(solution)	Sr–N	2.57(2)	6	EXAFS
H_2O(solution)	Ba–O	2.81(3)	8	X-ray diffraction, EXAFS
H_2O(solid)	Ba–O	2.79(1)[a]	8	X-ray crystallography
DMSO(solution)	Ba–O	2.76(1)	6	X-ray diffraction
Pyridine(solution)	Ba–N	2.78(3)	6	EXAFS

[a] Mean value.

and barium ions in solution is given in Table 11. For the aqueous solutions both our LAXS and EXAFS data are consistent with eight-coordination, although it is not possible from these results to determine the coordination geometry in solution, i.e. if the water molecules on the average have an antiprismatic arrangement around the strontium and barium ions as in the solid octahydrated hydroxides $Ba(H_2O)_8(OH)_2$ and $Sr(H_2O)_8(OH)_2$. The rather well-defined second coordination spheres in the solid $Ba(H_2O)_8(OH)_2$ and $Sr(H_2O)_8(OH)_2$ compounds, comprising 24 oxygen atoms (O^{II}) hydrogen-bonded to the octahydrated ions, are found to be very diffuse in solution. The lower number (ca. 13) and the large distribution of the second sphere water molecules around a similar $M \cdots O^{III}$ distance as in the solid compounds, correspond to the expected greater conformational flexibility of the first-sphere aqua ligands in solution, as is also indicated by the about 2–3 water molecules found to be present at about 4.1 Å from the Sr^{2+} and Ba^{2+} ions.

Despite the large variation in hydration numbers from four to eight for the alkaline earth metal ions, an almost linear correlation is found between the hydration enthalpies and the inverse of the metal-oxygen distances in solution. This is taken as an indication of a cancellation of higher order terms in the contribution from the binding energies of the hydrated ions. The correlation is used to estimate a hydration number of 8.5 ± 0.5 for the Ra^{2+} ion.

The Sr^{2+} and Ba^{2+} ions coordinate six dimethyl sulfoxide molecules in solution; as expected for hard electron-pair acceptors *via* the oxygen atom. The metal ion-oxygen bond distances are shorter than in water, ca. 0.09 and 0.05 Å for strontium and barium, respectively, and are consistent with six-coordination. The distinct $M \cdots S$ distances obtained by the LAXS method correspond to average M–O–S angles of 136(1)° for both ions. The relatively short M–N bond lengths obtained for the solvated ions in pyridine solution are also in agreement with (as discussed above) a probable solvation number of six for both the strontium and barium ions.

Acknowledgements

The support given by the Swedish Natural Science Research Council to this investigation and by the U.S. Department of Basic Energy Science, Division of Chemical/Material Science to the EXAFS measurements at the SSRL, is gratefully acknowledged. One of us (MS) wishes to thank the Institute for Molecular Science, Okazaki, Japan, for a visiting associate professorship. We are grateful to Drs. Graham N. George and Ingrid Pickering for providing us with the EXAFSPAK software, Dr. Per Persson for valuable advice in analysing the EXAFS data, and Mr. Ernst Hansen for skillful technical assistance.

[1] M. Sandström, I. Persson, and P. Persson, Acta Chem. Scand. **44,** 653 (1990).
[2] S. Ahrland, J. Chatt, and N. R. Davies, Quart. Rev., Chem. Soc. **11,** 265 (1958).
[3] R. G. Pearson, in: The Concept of the Chemical Bond (Z. B. Maksić, ed.), Springer-Verlag, Berlin 1990, Chapter 2.
[4] M. Johnsson and I. Persson, Inorg. Chim. Acta **127,** 15, 25, 43 (1987).
[5] D. Inerowicz, L. Wei, and I. Persson, J. Chem. Soc., Faraday Trans. **90,** 2223 (1994).
[6] M. Chaudhry, K. C. Dash, E. Kamienska-Piotrowicz, Y. Kinjo, and I. Persson, J. Chem. Soc., Faraday Trans. **90,** 2235 (1994).
[7] M. Chaudhry, Y. Kinjo, and I. Persson, J. Chem. Soc., Faraday Trans. **90,** 2683 (1994).
[8] (a) Y. Marcus, Pure Appl. Chem. **55,** 977 (1983). (b) Ibid. **57,** 1103 (1985), and references therein.
[9] R. Åkesson, M. Sandström, C. Stålhandske, and I. Persson, Acta Chem. Scand. **45,** 16 (1991).
[10] H. Ohtaki and T. Radnai, Chem. Rev. **93,** 1157 (1993), and references therein.

[11] G. W. Neilson and R. D. Broadbent, Chem. Phys. Lett. **167,** 429 (1990).
[12] (a) G. Johansson and H. Yokoyama, Inorg. Chem. **29,** 2460 (1990). (b) G. Johansson, Adv. Inorg. Chem. **39,** 159 (1992).
[13] (a) E. A. Stern, in: X-Ray Absorption: Principles, Applications, Techniques of EXAFS, SEXAFS and XANES (D. C. Koningsberger and R. Prins, eds.), Wiley, New York 1988, Chapter 1. (b) E. D. Crozier, J. J. Rehr, and R. Ingalls, Ibid., Chapter 9.2. (c) D. E. Sayers and B. A. Bunker, Ibid., Chapter 6.
[14] G. Johansson and M. Sandström, Chem. Scrip. **4,** 195 (1973), and references therein.
[15] J. Blixt, J. Glaser, J. Mink, I. Persson, P. Persson, and M. Sandström, J. Amer. Chem. Soc. Accepted for publication.
[16] Handbook of Spectroscopy (J. W. Robinson, ed.), CRC Press, Boca Raton, Florida 1991, Chapter 3.
[17] J. J. Rehr, Japan. J. Appl. Phys. **32,** 8 (1993).
[18] H. G. Smith, Acta Cryst. **6,** 604 (1953).
[19] H. Manohar and Z. Ramaseshan, Z. Kristallogr. **119,** 357 (1964).
[20] M. Sacerdoti, V. Bertolasi, V. Ferretti, and C. A. Accorsi, Z. Kristallogr. **192,** 111 (1990).
[21] R. Caminiti, A. Musinu, G. Paschina, and G. Pinna, J. Appl. Cryst. **15,** 482 (1982).
[22] G. R. Hedwig and A. J. Parker, J. Amer. Chem. Soc. **96,** 6589 (1974).
[23] M. Broul, J. Nyvlt, and O. Söhnel, Solubility in Inorganic Two-Component Systems, Elsevier, Amsterdam 1981, pp. 98, 519.
[24] G. Berggren and A. Brown, Acta Chem. Scand. **25,** 14 (1971).
[25] A. C. T. North, D. C. Phillips, and F. Scott Mathews, Acta Cryst. **A 24,** 351 (1964).
[26] G. M. Sheldrick, SHELXTL PLUS 1992, Program for Crystal Structure Determination, University of Göttingen, Germany.
[27] International Tables of Crystallography, 3rd ed., Kluwer Academic Publishers, Dordrecht 1992. (a) Vol. C (A. J. C. Wilson, ed.). (b) Vol. A (T. Hahn, ed.).
[28] G. Johansson, Acta Chem. Scand. **20,** 553 (1966); **25,** 2787 (1971).
[29] M. Molund and I. Persson, Chem. Scr. **25,** 197 (1985).
[30] M. E. Milberg, J. Appl. Phys. **29,** 64 (1978).
[31] G. N. George and I. J. Pickering, EXAFSPAK – A Suite of Computer Programs for Analysis of X-Ray Absorption Spectra, SSRL, Stanford University, CA., U.S.A., 1993.
[32] (a) P. Kuske, B. Engelen, J. Henning, and H. D. Lutz, Z. Kristallogr. **183,** 319 (1988). (b) H. D. Lutz, P. Kuske, and J. Henning, J. Mol. Struct. **176,** 149 (1988).
[33] (a) G. A. Jeffrey, in: Accurate Molecular Structures, IUCr Monographs on Crystallography, No. 1 (A. Domenicano and I. Hargittai, eds.), Oxford University Press, Oxford, U.K. 1992, Chapter 11; (b) K. N. Trueblood, Ibid., Chapter 8.
[34] G. H. Stout and L. H. Jensen, X-Ray Structure Determination, Wiley-Interscience, New York, 2nd ed. 1989, Chapter 19.
[35] (a) H. D. Lutz, Th. Kellersohn, and Th. Vogt, Acta Cryst. **C 46,** 361 (1990). (b) H. D. Lutz, W. Eckers, G. Schneider, and H. Haeuseler, Spectrochim. Acta **37 A,** 561 (1981).
[36] H. D. Lutz, Struct. Bond. **69,** 97 (1988).
[37] R. E. Gerkin, W. J. Reppart, and E. H. Appelman, Acta Cryst. **C 44,** 960 (1988).
[38] K. Mereiter and A. Preisinger, Acta Cryst. **C 44,** 1178 (1988).
[39] O. Kristiansson, A. Eriksson, and J. Lindgren, Acta Chem. Scand. **A 38,** 609, 613 (1984).
[40] P.-Å. Bergström and J. Lindgren, Inorg. Chem. **31,** 1529 (1992).
[41] J. Lindgren, O. Kristiansson, and C. Paluszkiewicz, in: Interactions of Water in Ionic and Non-Ionic Hydrates (H. Kleeberg, ed.), Springer-Verlag, Berlin 1987, p. 43.
[42] (a) H. Einspahr and C. E. Bugg, Acta Cryst. **B 36,** 264 (1980). (b) O. Carugo, K. Djinović, and M. Rizzi, J. Chem. Soc., Dalton Trans. 2127 (1993).
[43] B. Berglund, J. Lindgren, and J. Tegenfeldt, J. Mol. Struct. **43,** 179 (1987).
[44] (a) M. Sandström and I. Persson, Acta Chem. Scand. **A 32,** 95 (1978). (b) M. Sandström, Ibid., 519.
[45] G. Nieuwpoort, G. C. Verschoor, and J. Reedijk, J. Chem. Soc., Dalton Trans. 531 (1983).
[46] S. Ahrland, E. Hansson, Å. Iverfeldt, and I. Persson, Acta Chem. Scand. **A 35,** 275 (1981).
[47] R. D. Shannon, Acta Cryst. **A 32,** 751 (1976).
[48] G. Johansson and M. Sandström, Acta Chem. Scand. **A 41,** 113 (1987).
[49] I. Persson, Acta Chem. Scand. **A 36,** 7 (1982).
[50] G. Smith, E. J. O'Reilly, C. H. L. Kennard, and A. H. White, J. Chem. Soc., Dalton Trans. 1184 (1977).
[51] R. J. Doedens and L. F. Dahl, J. Amer. Chem. Soc. **88,** 4847 (1966).
[52] H. Ohtaki, T. Yamaguchi, and M. Maeda, Bull. Chem. Soc. Japan **47,** 2197 (1974).
[53] Y. Agnus, M. Labarelle, R. Louis, and B. Metz, Acta Cryst. **C 50,** 536 (1994).
[54] F. A. Cotton, L. M. Daniels, and C. A. Murillo, Inorg. Chem. **32,** 4868 (1993).
[55] R. Åkesson, L. G. M. Pettersson, M. Sandström, P. E. M. Siegbahn, and U. Wahlgren, J. Phys. Chem. **96,** 10773 (1992).
[56] Y. Marcus, Ion Solvation, Wiley Chicester 1985, p. 306.
[57] B. E. Conway, Ionic Hydration in Chemistry and Biophysics, Elsevier, Amsterdam 1981, Chapters 14, 15, 25.
[58] T. W. Swaddle and M. K. S. Mak, Can. J. Chem. **61,** 473 (1983).
[59] T. Kellersohn, R. G. Delaplane, and I. Olovsson, Acta Cryst. **B 50,** 316 (1994).
[60] (a) K. Hashimoto, N. Yoda, and S. Iwata, Chem. Phys. **116,** 193 (1987). (b) C. W. Bock and J. P. Glusker, Inorg. Chem. **32,** 1242 (1993).
[61] D. W. Smith, J. Chem. Educ. **54,** 540 (1977).
[62] T. Yamaguchi, H. Ohtaki, E. Spohr, G. Pálinkás, K. Heinzinger, and M. M. Probst, Z. Naturforsch. **A 41,** 1175 (1986).
[63] J. O'M. Bockris and A. K. N. Reddy, Modern Electrochemistry, Plenum, New York 1974, Vol. 1, Chapter 2.
[64] A. A. Rashin and B. Honig, J. Phys. Chem. **89,** 5588 (1985).
[65] J. R. Bontha and P. N. Pintauro, J. Phys. Chem. **96,** 7778 (1992).
[66] R. Åkesson, L. G. M. Pettersson, M. Sandström, and U. Wahlgren, J. Amer. Chem. Soc. **116,** 8691 (1994).